Two Organic–Inorganic Hybrids Assembled from Transition–Metal Complexes and Keggin-Type Silicotungstates

Jie Luo, Jian-Cai Liu, Bo Shao, Li-Juan Chen & Jun-Wei Zhao

Journal of Cluster Science
Including Nanoclusters and Nanoparticles

ISSN 1040-7278
Volume 26
Number 6

J Clust Sci (2015) 26:2005-2022
DOI 10.1007/s10876-015-0899-1

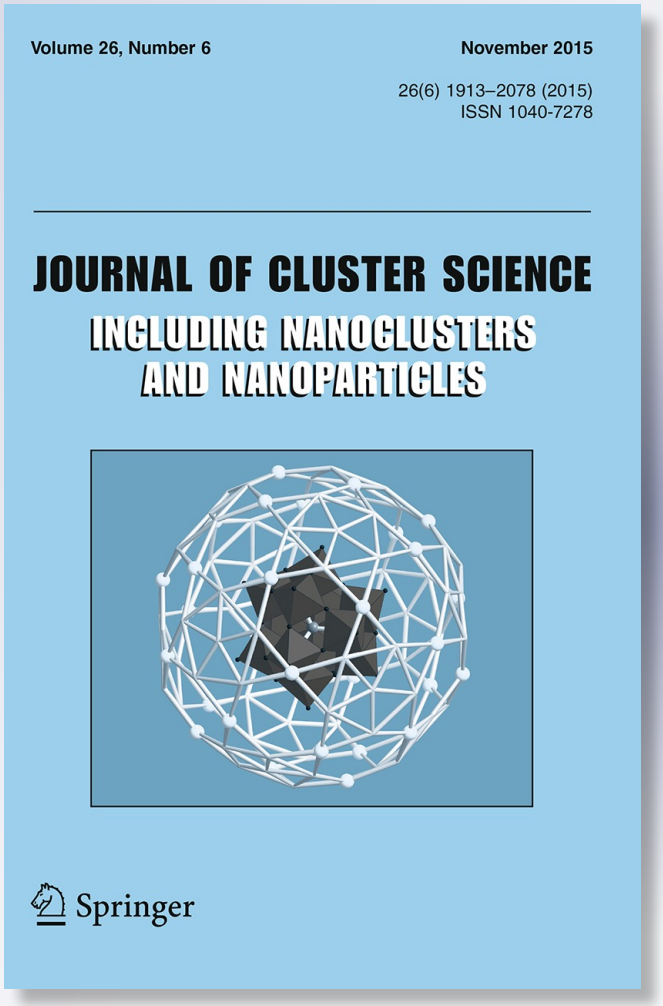

Springer

Your article is protected by copyright and all rights are held exclusively by Springer Science +Business Media New York. This e-offprint is for personal use only and shall not be self-archived in electronic repositories. If you wish to self-archive your article, please use the accepted manuscript version for posting on your own website. You may further deposit the accepted manuscript version in any repository, provided it is only made publicly available 12 months after official publication or later and provided acknowledgement is given to the original source of publication and a link is inserted to the published article on Springer's website. The link must be accompanied by the following text: "The final publication is available at link.springer.com".

Author's personal copy

J Clust Sci (2015) 26:2005–2022
DOI 10.1007/s10876-015-0899-1

ORIGINAL PAPER

Two Organic–Inorganic Hybrids Assembled from Transition–Metal Complexes and Keggin-Type Silicotungstates

Jie Luo[1] · Jian-Cai Liu[1] · Bo Shao[1] · Li-Juan Chen[1] · Jun-Wei Zhao[1]

Received: 8 April 2015 / Published online: 4 July 2015
© Springer Science+Business Media New York 2015

Abstract By introducing rigid aromatic N-ligands to the lacunary silicotungstate system under hydrothermal conditions, two new Keggin-type polyoxotungstate hybrids with copper–organic complexes $[Cu(phen)(H_2O)_2]_2[Cu(phen)_2]_2[\alpha\text{-}SiW_{12}O_{40}]_2{\cdot}4H_2O$ (**1**) and $[Cu(4,4'\text{-bpy})]_3H[\alpha\text{-}SiW_{12}O_{40}]{\cdot}3\ H_2O$ (**2**) (phen = 1,10-phenanthroline, 4,4′-bpy = 4,4′-bipyridine) have been made and characterized by elemental analysis, IR spectra and single-crystal X-ray diffraction. The common architectural feature of **1** and **2** is that both comprise the plenary Keggin-type $[\alpha\text{-}SiW_{12}O_{40}]^{4-}$ polyoxoanions modified by Cu–organic fragments containing various organic ligands. It should be pointed out that $\{[Cu(phen)\ (H_2O)_2][\alpha\text{-}SiW_{12}O_{40}]\}^{2+}$ and $\{[Cu(phen)_2][\alpha\text{-}SiW_{12}O_{40}]\}^{2+}$ building units in **1** are alternately held together into an infinite 1-D chain fashion while the most striking characteristic of **2** is that two types of $\{-4,4'\text{-bpy–Cu–}\ 4,4'\text{-bpy–Cu–}\}_n$ 1-D polymeric chains are combined together by hexadentate $[\alpha\text{-}SiW_{12}O_{40}]^{4-}$ polyoxoanions as the inorganic bridging ligands, giving birth to the aesthetic 3-D extended architecture. Moreover, electrochemical properties of **1** and **2** have been investigated.

Keywords Organic–inorganic hybrid · Silicotungstate · Electrochemical properties

Electronic supplementary material The online version of this article (doi:10.1007/s10876-015-0899-1) contains supplementary material, which is available to authorized users.

✉ Jun-Wei Zhao
zhaojunwei@henu.edu.cn

Li-Juan Chen
ljchen@henu.edu.cn

[1] Henan Key Laboratory of Polyoxometalate Chemistry, Institute of Molecule and Crystal Engineering, College of Chemistry and Chemical Engineering, Henan University, Kaifeng 475004, Henan, China

Author's personal copy

Introduction

Polyoxometalates (POMs), as a remarkable class of inorganic metal oxide clusters, have received much attention not only because of their unrivalled electronic and structural diversities, but also on account of their multiple applications such as catalysis, medicine, magnetism and materials science [1–7]. As well known, some POMs are often easily accessible, own high-negative charges, exhibit much stronger coordination ability through exposing many active surface coordination sites and are usually utilized as the preferred candidates for the design and fabrication of various transition-metal (TM) or lanthanide (Ln) containing POM hybrids [8–13]. Therefore, it has aroused great interest and numerous fascinating TM or Ln containing POMs have been extensively discovered in recent years [14–20]. In particular, the versatile functionalization of saturated Keggin-type $[\alpha\text{-}SiW_{12}O_{40}]^{4-}$ polyoxoanions (POAs) have led to the great possibility for the structural diversity of silicotungstates (STs) and make them stand out from other multitudinous TM or Ln including POMs. It's noteworthy that the $[\alpha\text{-}SiW_{12}O_{40}]^{4-}$ POAs can readily degrade and transform to mono-, di-, tri-, even tetra-vacant Keggin derivatives and can also isomerize to the α-, β-, or γ-framework such as $[\alpha\text{-}SiW_{11}O_{39}]^{8-}$, $[\beta_2\text{-}SiW_{11}O_{39}]^{8-}$, $[\gamma\text{-}SiW_{10}O_{36}]^{8-}$, $[\alpha\text{-}SiW_9O_{34}]^{10-}$, $[\beta\text{-}SiW_9O_{34}]^{10-}$, $[\beta\text{-}SiW_8O_{31}]^{10-}$ and $[\gamma\text{-}SiW_8O_{31}]^{10-}$. Some representative examples are listed as follows: Mizuno synthesized a dicopper-substituted γ-Keggin ST (TBA = tetra-n-butylammonium) [21] by treating $[\gamma\text{-}SiW_{10}O_{36}]^{8-}$ with Cu^{2+} in the presence of NaN_3; Kortz and co-workers showed the interaction of Ni^{2+} with $[\gamma\text{-}SiW_{10}O_{36}]^{8-}$ leading to a novel dimeric ST $K_{12}[\{\beta\text{-}SiNi_2W_{10}O_{36}(OH)_2(H_2O)\}_2]\cdot 20H_2O$ [22]; Cronin et al. communicated a mixed-valence manganese double-cubane cluster $K_{18}\left[Mn_2^{III}Mn_4^{III}(\mu_3-O)_2(H_2O)_4(B-\beta-SiW_8O_{31})(B-\beta-SiW_9O_{34})(\gamma-SiW_{10}O_{36})\right]\cdot 40H_2O$ [23]; Recently, Wang et al. reported a new ST-based $\{Mn_{12}\}$ complex $K_8Na_{10}\left\{\left[Mn_2^{IV}Mn_6^{III}Mn_4^{II}(\mu_3-O)_6(\mu-OH)_4(H_2O)_2(CO_3)_6\right][B-\beta-SiW_6O_{26}]_2\right\}\cdot 30H_2O$ exhibiting the largest known manganese nuclearity and the most manganese valence states in the POM-based single-molecule magnet family, in which the in situ formed discrete $\{SiW_6O_{26}\}$ moiety is observed for the first time in POM chemistry [24]. The above results suggest that the intrinsic properties and the reaction environments of the precursors have a great influence on the nature of the in situ generated build block libraries and ultimately, the final architectures of outcomes.

The manifold structural types of defect ST precursors and the accessibility of abundant initial materials have driven chemists to search and exploit their Ln-containing derivatives, even going so far as to TM–Ln heterometallic derivatives. Nevertheless, reports on TM–Ln heterometallic STs are very limited in contrast to a large number of already reported TM-containing STs [21–24] and Ln-including STs [25–31]. For instance, Wang's group successively reported several 3d–4f heterometallic STs $[\{Ce(H_2O)_7\}_2Mn_4Si_2W_{18}O_{68}(H_2O)_2]^{6-}$ [32], $\{Nd_2(H_2O)_{12}Cu_4(H_2O)_2(SiW_9O_{34})_2\}^{6-}$ [33], $[K_9Ln_6Fe_6(H_2O)_{12}(SiW_{10}O_{38})_6]^{26-}$ (Ln = Dy^{III}, Tb^{III}) [34], $[\{Cu(en)_2\}_9\{K_4Na_2[Dy(SiW_{11}O_{39})_2]_2\}]^{2-}$ [35] and $\left[\left\{Dy^{III}Mn_4^{III}(\mu_3-O)_2(\mu_2-OH)_2(H_2O)(CO_3)\right\}(\beta-SiW_8O_{31})_2\right]^{13-}$ [36]. Mialane et al. obtained unprecedented $\{LnCu_3(OH)_3O\}$-cubane (Ln = La^{III}, Gd^{III}, Eu^{III}) inserted monovacant

Author's personal copy

$[\alpha\text{-}SiW_{11}O_{39}]^{8-}$ derivatives [37] and an inorganic 1-D double-chain derivative $[(\gamma\text{-}SiW_{10}O_{36})_2(Cr(OH)(H_2O))_3(La(H_2O)_7)_2]^{4-}$ [38]. Besides, Su, Luban and Yang also reported some TM–Ln heterometallic STs such as $[Cu(en)_2H_2O]_3[(\alpha\text{-}SiW_{11}O_{39})Ln(H_2O)(\eta^2,\mu\text{-}1,1)CH_3COO]\cdot 3.5H_2O$ (Ln = Sm^{III}, Nd^{III}) [39], $[Cu(en)_2H_2O]_8[Cu(en)_2]_3[\{(\alpha\text{-}SiW_{11}O_{39})Ce(H_2O)(\eta^2,\mu\text{-}1,1)CH_3COO\}_4]^{2-}$ [39], $\{[(A\text{–}\beta\text{–}SiW_9O_{34})_2]Ce_4^{IV}O_2(CH_3COO)_2]\cdot[(A\text{–}\beta\text{–}SiW_9O_{34})Mn_3^{III}Mn^{IV}O_3(CH_3COO_3)]_2\}^{22-}$ [40] and $[Cu(en)_2(H_2O)]_2[Tb(\alpha\text{-}HSiW_{11}O_{39})(H_2O)_3]\cdot 12H_2O$ (en = ethylenediamine) [41]. It's noteworthy that Peng's group successfully yielded two unwonted 4d–4f heterometallic STs $\{[Ag\{Ag_2(H_2O)_4\}\{Ln(H_2O)_6\}_2H \subset \{SiW_{11}Ln(H_2O)_4O_{39}\}_2]\cdot nH_2O$ (Ln = Ce^{III}, n = 7; Ln = Pr^{III}, n = 3), which represent the highest number of connected metal atoms to any mono-lacunary Keggin anion [42].

Encouraged by the aforementioned results, our group has also performed a systematic investigation with the aim of understanding the assembly of TM, Ln cations with ST precursors in the presence of organic ingredients so as to obtain novel organic–inorganic hybrid TM–Ln heterometallic STs. Nevertheless, in the TM–Ln–POM system, the oxyphilic Ln cations and relatively less active TM cations in the same reaction system create competition for highly negative POAs. Besides, it's difficult to control the encapsulated positions via grafting TM or Ln complexes onto the POMs surfaces. However, these two major drawbacks can be to some extent overcome by the hydrothermal method as well as using suitable TM, Ln cations and functional ligands to embellish POMs. In an attempt to develop an approach to this goal, we opted to use the trivacant Keggin $[\alpha\text{-}SiW_9O_{34}]^{10-}$ as the precursor to react with Cu^{2+}, Ln cations and flexible aliphatic organoamine ligands to construct novel 3d–4f heterometallic organic–inorganic hybrids based on the following ideas: (i) the Cu^{2+} ion can adopt several coordination modes (square, trigonal bipyramid, square pyramid and octahedron) and the axial distortion as a result of the Jahn–Teller effect will be beneficial to overcome steric hindrance and lead to multi-dimensional organization via long Cu–O bonds; (ii) some N-containing organic ligands have proved to be good donors to coordinate to electrophilic TM cations, readily generating TM complexes that availably work as connectors to build high-dimensional structures. Eventually, we obtained some 3d–4f heterometallic STs from discrete to high-dimensional structures [43–47]. A library of novel 1-D organic–inorganic double-chain 3d−4f heterometallic STs $[Cu(dap)_2(H_2O)]_2\{Cu(dap)_2[\alpha\text{-}H_2SiW_{11}O_{39}Ln(H_2O)_3]_2\}\cdot xH_2O$ (Ln = Ce^{III}, Gd^{III}, Er^{III}, x = 9; Ln = Pr^{III}, Nd^{III}, Sm^{III}, Eu^{III}, x = 10; Ln = Tb^{III}, Dy^{III}, x = 8) [44] and $[Cu(dap)_2(H_2O)]_2\{Cu(dap)_2[\alpha\text{-}H_2SiW_{11}O_{39}Y(H_2O)_2]_2\}\cdot 10H_2O$ were reported by us [47]. Subsequently, several 3-D 3d–4f heterometallic hybrids $\{[Cu(en)_2(H_2O)][Cu(en)_2]_nLn[(\alpha\text{-}SiW_{11}O_{39})_2]\}^{m-}$ [Ln = Pr^{III}, n = 2, m = 7; Ln = Sm^{III}, n = 3, m = 5] [43] and $\{[Cu(dap)_2(H_2O)][Cu(dap)_2]_{4.5}[Ln(\alpha\text{-}SiW_{11}O_{39})_2]\}^{3-}$ (Ln = Sm^{III}, Dy^{III}, Gd^{III}) [45] were made. As a part of our continuous work, when we extended flexible aliphatic organoamine ligands to rigid aromatic N-ligands, unexpectedly, two organic–inorganic hybrids assembled from TM complexes and Keggin-type ST units $[Cu(phen)(H_2O)_2]_2[Cu(phen)_2]_2[\alpha\text{-}SiW_{12}O_{40}]_2\cdot 4H_2O$ (**1**) and $[Cu(4,4'\text{-bpy})]_3H[\alpha\text{-}SiW_{12}O_{40}]\cdot 3H_2O$ (**2**) (phen = 1,10-phenanthroline, 4,4′-bpy = 4,4′-bipyridine) have been obtained. **1** displays a 1-D infinite chain

Author's personal copy

architecture and **2** exhibits an intriguing 3-D framework. What's more, the electrochemical properties of **2** have been investigated.

Experimental

Materials and Methods

The starting material $Na_{10}[\alpha\text{-}SiW_9O_{34}]\cdot 18H_2O$ was synthesized according to the published procedure [48] and confirmed by IR spectra. All other chemical reagents were purchased from commercial sources and used without further purification. Elemental analyses (C, H and N) were conducted on a Perkin–Elmer 2400-II CHNS/O analyzer. Inductively coupled plasma atomic emission spectrometry (ICP-AES) was carried out on a Perkin–Elmer Optima 2000 ICP-AES spectrometer. IR spectra were recorded on a Nicolet FT–IR 360 spectrometer using KBr pellets in the range of 4000–400 cm^{-1}. Cyclic voltammograms were carried out on a CS electrochemical workstation (Wuhan Corrtest Instrument Co. LTD) at room temperature. A conventional three-electrode system was used. Platinum gauze was used as a counter electrode, and an Ag/AgCl electrode was referenced. Chemically bulk-modified carbon paste electrodes (CPEs) were used as working electrodes. Thermogravimetric (TG) analysis was performed under a N_2 atmosphere on a Mettler–Toledo TGA/SDTA 851^e instrument with a heating rate of 10 °C min^{-1} from 25 to 1000 °C.

$$\text{Synthesis of } \left[Cu(phen)(H_2O)_2\right]_2\left[Cu(phen)_2\right]_2[\alpha - SiW_{12}O_{40}]_2\cdot 4H_2O \qquad (1)$$

A mixture of $Na_{10}[\alpha\text{-}SiW_9O_{34}]\cdot 18H_2O$ (0.150 g, 0.0539 mmol), $CuCl_2\cdot 2H_2O$ (0.190 g, 1.114 mmol), $SmCl_3$ (0.050 g, 0.195 mmol), phen (0.030 g, 0.151 mmol), 2,3-pyrazine dicarboxylic acid (2,3-pdca) (0.030 g, 0.178 mmol), H_2O (10 mL, 554 mmol) and ethyl alcohol (5 mL, 85.9 mmol) was stirred for 4 h in air, sealed in a 25 mL Teflon-lined steel autoclave, kept at 110 °C for 5 days and then slowly cooled to room temperature. Green prismatic crystals were collected by filtration, washed with distilled water and dried in air at ambient temperature. Yield: ca. 28 % (based on $Na_{10}[\alpha\text{-}SiW_9O_{34}]\cdot 18H_2O$). Element analysis (%) calcd. for $C_{72}H_{64}Cu_4N_{12}O_{88}Si_2W_{24}$ (**1**): C, 11.96; H, 0.89; N, 2.33, Si, 0.78, Cu, 3.52, W, 61.04. Found: C, 12.01; H, 0.86; N, 2.30, Si, 0.86, Cu, 3.38, W, 60.32.

$$\text{Synthesis of } [Cu(4,4\prime - bpy)]_3H[\alpha - SiW_{12}O_{40}]\cdot 3H_2O \qquad (2)$$

A mixture of $Na_{10}[\alpha\text{-}SiW_9O_{34}]\cdot 18H_2O$ (0.130 g, 0.0467 mmol), $CuCl_2\cdot 2H_2O$ (0.180 g, 1.055 mmol), $PrCl_3$ (0.048 g, 0.194 mmol), biimidazole (biim) (0.050 g, 0.373 mmol), 4,4′-bpy (0.030 g, 0.192 mmol), H_2O (6 mL, 332 mmol) was stirred for 3 h in air, sealed in a 25 mL Teflon-lined steel autoclave, kept at 160 °C for 5 days and then slowly cooled to room temperature. Black cubic crystals were collected by filtration, washed with distilled water and dried in air at ambient

Author's personal copy

temperature. Yield: ca. 25 % (based on $Na_{10}[\alpha\text{-}SiW_9O_{34}]\cdot 18H_2O$). Element analysis (%) calcd. for $C_{30}H_{31}Cu_3N_6O_{43}SiW_{12}$ (**2**): C, 10.04; H, 0.87; N, 2.34, Si, 0.78, Cu, 5.31, W, 61.48. Found: C, 10.13; H, 0.96; N, 2.27, Si, 0.91, Cu, 5.18, W, 60.74.

X-ray Crystallography

Intensity data collections for **1** and **2** were carried out on a Bruker APEX-II CCD diffractometer using graphite monochromatized Mo Kα radiation ($\lambda = 0.71073$ Å) at 296 (2) K. Direction methods were used to solve the structures and to locate the heavy atoms using the SHELXTL–97 program package [49, 50]. The remaining atoms were found from successive full-matrix least-squares refinements on F^2 and Fourier syntheses. Routine Lorentz polarization and empirical absorption corrections were applied. No H atoms associated with water molecules were from the difference Fourier map. Positions of the H atoms attached to C and N atoms were geometrically placed. All H atoms were refined isotropically as a riding mode using the default SHELXTL parameters. All non-H atoms except for some O, C, N atoms and water molecules were refined anisotropically. Crystal data and structure refinements for **1** and **2** are listed in Table 1.

Preparation of 1-CPE and 2-CPE

A **1**-modified carbon paste electrode (**1**-CPE) was fabricated as follows: 30 mg of graphite powder and 10 mg of **1** were mixed and ground together by an agate mortar and pestle to achieve a uniform mixture, and then 0.05 mL of paraffin oil was added with stirring. The homogenized mixture was packed into a glass tube with a 3.0 mm inner diameter, and the tube surface was wiped with paper. Electrical contact was established with a copper rod through the back of the electrode. **2**-CPE was prepared in the same way.

Results and Discussion

Synthesis

In this paper, **1** and **2** have been synthesized by the $Na_{10}[\alpha\text{-}SiW_9O_{34}]\cdot 18H_2O$ precursor under hydrothermal conditions. Obviously, the tri-vacant $[\alpha\text{-}SiW_9O_{34}]^{10-}$ POA in the precursor finally was transformed to the saturated $[\alpha\text{-}SiW_{12}O_{40}]^{4-}$ POA in the formation of **1** and **2**. As we know, the $[\alpha\text{-}SiW_{12}O_{40}]^{4-}$ POAs can easily degrade and transform to lacunary Keggin derivative species with increasing pH, therefore, the transformation of $[\alpha\text{-}SiW_9O_{34}]^{10-} \rightarrow [\alpha\text{-}SiW_{12}O_{40}]^{4-}$ can be understandable. In addition, though $SmCl_3$ and 2,3-pdca in **1**, $PrCl_3$ and biim in **2** were used as starting materials in the reaction, they didn't appear in the final structures of **1** and **2**, the main reason of which is relevant to the fact that it is very difficult to simultaneously graft Cu^{2+} and Ln^{3+} ions to the surface of the $[\alpha\text{-}SiW_{12}O_{40}]^{4-}$ POAs because the positive charges of Cu^{2+} and Ln^{3+} ions are higher than the negative charge of $[\alpha\text{-}SiW_{12}O_{40}]^{4-}$ POAs. A series of parallel synthetic experiments

Author's personal copy

Table 1 Summary of crystallographic data for **1** and **2**

Compound	**1**	**2**
Formula	$C_{72}H_{64}Cu_4N_{12}O_{88}Si_2W_{24}$	$C_{30}H_{31}Cu_3N_6O_{43}SiW_{12}$
Formula weight	7228.09	3588.43
Crystal system	Monoclinic	Triclinic
Space group	*P*2(1)/c	*P*–1
a (Å)	19.573 (4)	10.887 (8)
b (Å)	19.354 (4)	11.591 (8)
c (Å)	17.367 (3)	13.279 (10)
α (°)	90	113.310 (13)
β (°)	95.715 (3)	96.328 (13)
γ (°)	90	95.334 (13)
Volume ($Å^3$)	6546 (2)	1512.3 (19)
Z	2	1
Density (g cm^{-3})	3.667	3.940
Absorption coefficient (mm^{-1})	21.744	23.866
F (000)	6408	1585
Limiting indices	$-14 \le h \le 23$	$-12 \le h \le 12$
	$-22 \le k \le 23$	$-13 \le k \le 8$
	$-20 \le l \le 20$	$-15 \le l \le 15$
Goodness-of-fit on F^2	1.075	1.068
Final *R* indices [$I > 2\sigma(I)$]	$R_1 = 0.0761$	$R_1 = 0.0927$
	$wR_2 = 0.1752$	$wR_2 = 0.2313$
R indices (all data)	$R_1 = 0.1392$	$R_1 = 0.1082$
	$wR_2 = 0.1938$	$wR_2 = 0.2433$
Largest diff. peak and hole (e $Å^{-3}$)	3.491 and −5.342	5.911 and −5.938

indicate that **1** and **2** could not be obtained when they were removed away from the reaction system. Similar phenomena have been previously encountered [51–53].

Structure Description

Single-crystal X-ray diffraction analysis reveals that **1** crystallizes in the monoclinic space group *P*2(1)/*c* and the molecular structural fragment of **1** is constructed from two saturated Keggin-type $[\alpha\text{-}SiW_{12}O_{40}]^{4-}$ POAs, two decorated $[Cu(phen)_2]^{2+}$ cations, two bridging $[Cu(phen)(H_2O)_2]^{2+}$ cations and four lattice water molecules (Fig. 1a). The $[\alpha\text{-}SiW_{12}O_{40}]^{4-}$ POA shows a classical α-Keggin configuration, whose structure can be regarded as a $\{W_{12}O_{36}\}$ shell encapsulating a $\{SiO_4\}$ core in its center. The central Si atom is surrounded by a cube of eight oxygen atoms with each oxygen site half-occupied. These eight oxygen atoms are all crystallographically disordered over two positions and similar disordered phenomena have been observed in the previous studies [54–56]. One interesting feature of **1** is that albeit both $[\alpha\text{-}SiW_{12}O_{40}]^{4-}$ POAs exhibit the typical α-Keggin structure, the central Si1 atom shows a slightly distorted eight-coordinated cubic geometry with Si–O

Author's personal copy

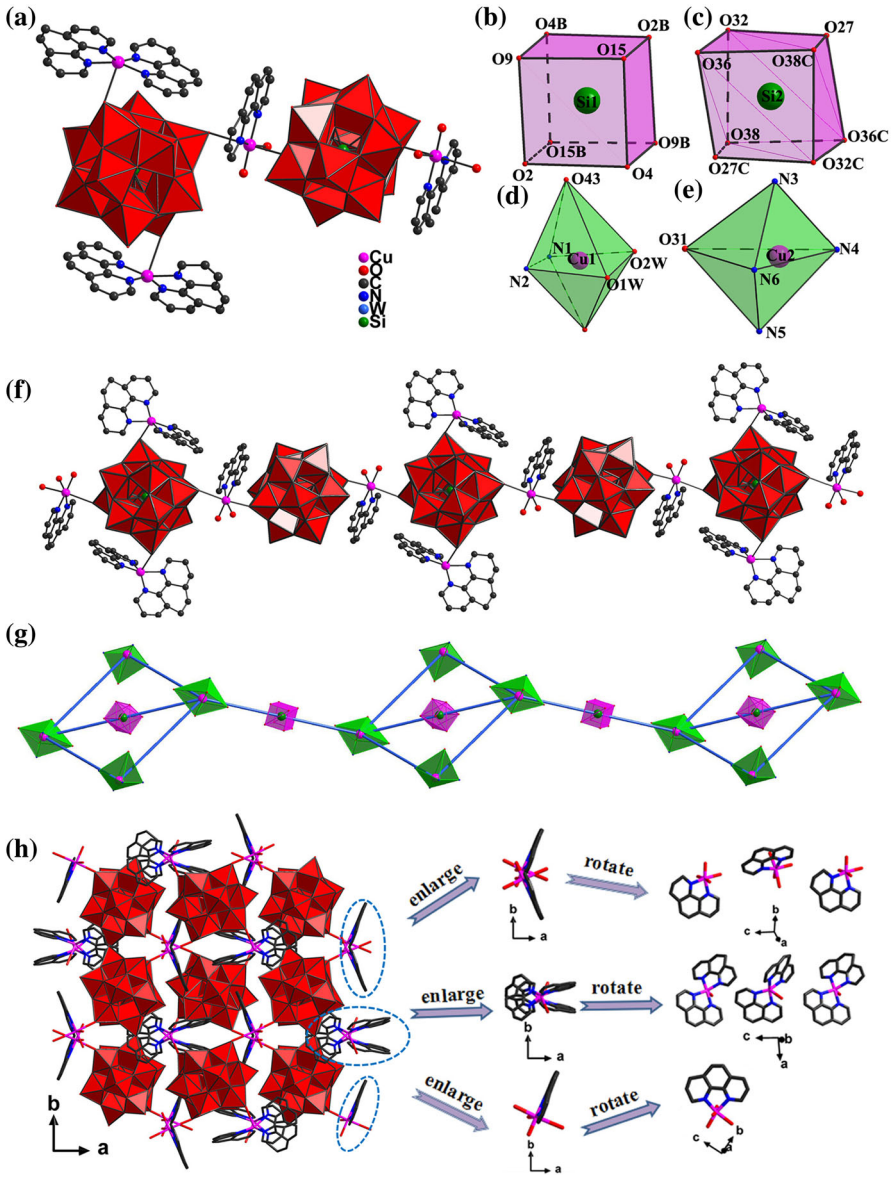

Fig. 1 **a** Combined ball-and-stick/polyhedral representation of the structural unit of **1** with the part labeling scheme. All the hydrogen atoms and lattice water molecules are omitted for clarity. **b** Coordination environment of the Si1 atom. **c** Coordination environment of the Si2 atom. **d** Coordination environment of the $Cu1^{2+}$ cation. **e** Coordination environment of the $Cu2^{2+}$ cation. **f** The 1-D chain architecture of **1**. **g** The simplified 1-D chain architecture and the parallelogram based on the closest Cu···Cu bonds. **h** View of the 3-D supramolecular architecture of **1**. The atoms with "A, B, C," in their labels are symmetrically generated symmetry code symmetry code: A: −x, 1 − y, 1 − z; B: −1 − x, −y, −1 − z; C: −x, 1 − y, −1 − z

Author's personal copy

distances ranging from 1.57(3) to 1.68(3) Å (Fig. 1b) whereas the central Si2 atom is also surrounded by a severely distorted cube of eight oxygen atoms with Si–O distances from 1.44(3) to 1.68(3) Å, which may arise from the non-ignorable interactions between cluster POAs and $[Cu(phen)(H_2O)_2]^{2+}$/$[Cu(phen)_2]^{2+}$ cations (Fig. 1c). In the $[\alpha\text{-Si1W}_{12}O_{40}]^{4-}$ POA, the W–O distances are in the range of 1.61(2)–2.48(3) Å and in the $[\alpha\text{-Si2W}_{12}O_{40}]^{4-}$ POA, the W–O distances are between 1.61(2) and 2.52(3) Å.

There are two crystallographically independent copper $[Cu1(phen)(H_2O)_2]^{2+}$ and $[Cu2(phen)_2]^{2+}$ cations in the asymmetric unit of **1** and both are located on the usual crystallographic sites having an occupancy of 1. The $[Cu1(phen)(H_2O)_2]^{2+}$ cation having a "4 + 2″ coordination geometry exhibits an elongated octahedral geometry constituted by two N atoms (N1, N2) from one phen ligand [Cu–N: 1.88(4)–1.97(2) Å] and two coordination water molecules [Cu–O: 1.85(4)–2.16(3) Å] in the equatorial plane and two O atoms from adjacent two $[\alpha\text{-SiW}_{12}O_{40}]^{4-}$ clusters for two axial positions [Cu–O: 2.30(2)–2.69(3) Å] (Fig. 1d). The $[Cu2(phen)_2]^{2+}$ cation that can be described as a "3 + 2" coordination geometry and adopts the trigonal bipyramid geometry defined by four N atoms from two phen ligands [Cu–N: 1.96(2) to 2.06(3) Å] and a long bond to a terminal O atom from a $[\alpha\text{-SiW}_{12}O_{40}]^{4-}$ cluster with Cu–O distance of 2.65(2) Å (Fig. 1e), in which N4, N6, O31 are located in the basal plane and N3, N5 occupy the axial positions.

It is interesting that $\{[Cu(phen)_2][\alpha\text{-SiW}_{12}O_{40}]\}^{2-}$ and$\{[Cu(phen)(H_2O)_2][\alpha\text{-SiW}_{12}O_{40}]\}^{2-}$ units are alternately connected through Cu–O bonds furnishing a 1-D liner chain architecture (Fig. 1f), in which the decorated $[Cu(phen)_2]^{2+}$ coordination cations are appended to two sides of the 1-D chain. The most distinctive feature of **1** is that each $[\alpha\text{-SiW}_{12}O_{40}]^{4-}$ cluster acting as a tetra-dentate inorganic ligand coordinates to two symmetrical $[Cu(phen)(H_2O)_2]^{2+}$ and two symmetrical $[Cu(phen)_2]^{2+}$ coordination cations via four terminal O atoms (O43, O43A, O31, O31A) resulting in a parallelogram with the edge length of ca. 10.48 × 9.58 Å based on the closest Cu···Cu distance (Fig. 1g). The parallelogram can accommodate one $[\alpha\text{-Si2W}_{12}O_{40}]^{4-}$ POA where the Si2 atom is just located at the inversion center. The parallelograms are further joined by $[\alpha\text{-Si1W}_{12}O_{40}]^{4-}$ POAs to generate a 1-D metal–organic chain, in which the $[\alpha\text{-SiW}_{12}O_{40}]^{4-}$ POA as a bridging inorganic component is extremely indispensable. The similar phenomenon is encountered in $[Cu(bpp)_2][H_2PW_{12}O_{40}]\cdot 2H_2O$ with a pseudo-grid structure built from supramolecular parallelograms [57]. The weak interactions [Cu···O = 2.65(2), 2.69(3) Å] between the $Si2W_{12}$ clusters and the Cu^{2+} cations make great contribution to stability of the crystal structure. Obviously, The $[\alpha\text{-Si2W}_{12}O_{40}]^{4-}$ cluster is worked as a tetradentate ligand connecting two $[Cu(phen)(H_2O)_2]^{2+}$ and two $[Cu(phen)_2]^{2+}$ cations whereas the $[\alpha\text{-Si1W}_{12}O_{40}]^{4-}$ cluster is served as a didentate ligand covalently bonding to two $[Cu(phen)(H_2O)_2]^{2+}$ cations. What's more, the 3-D supramolecular architecture of **1** can be constructed through face-to-face π···π stacking interactions between neighboring phen ligands (Fig. 1h).

X-ray diffraction analysis reveals that **2** crystallizes in the triclinic space group *P*–1, and the molecular structural unit of **2** consists of a saturated Keggin-type $[\alpha\text{-SiW}_{12}O_{40}]^{4-}$ POA, three $[Cu(4,4'\text{-bpy})]^{+}$ cations, one proton and three lattice water molecules (Fig. 2a). The $[\alpha\text{-SiW}_{12}O_{40}]^{4-}$ POA also exhibits a typical

Author's personal copy

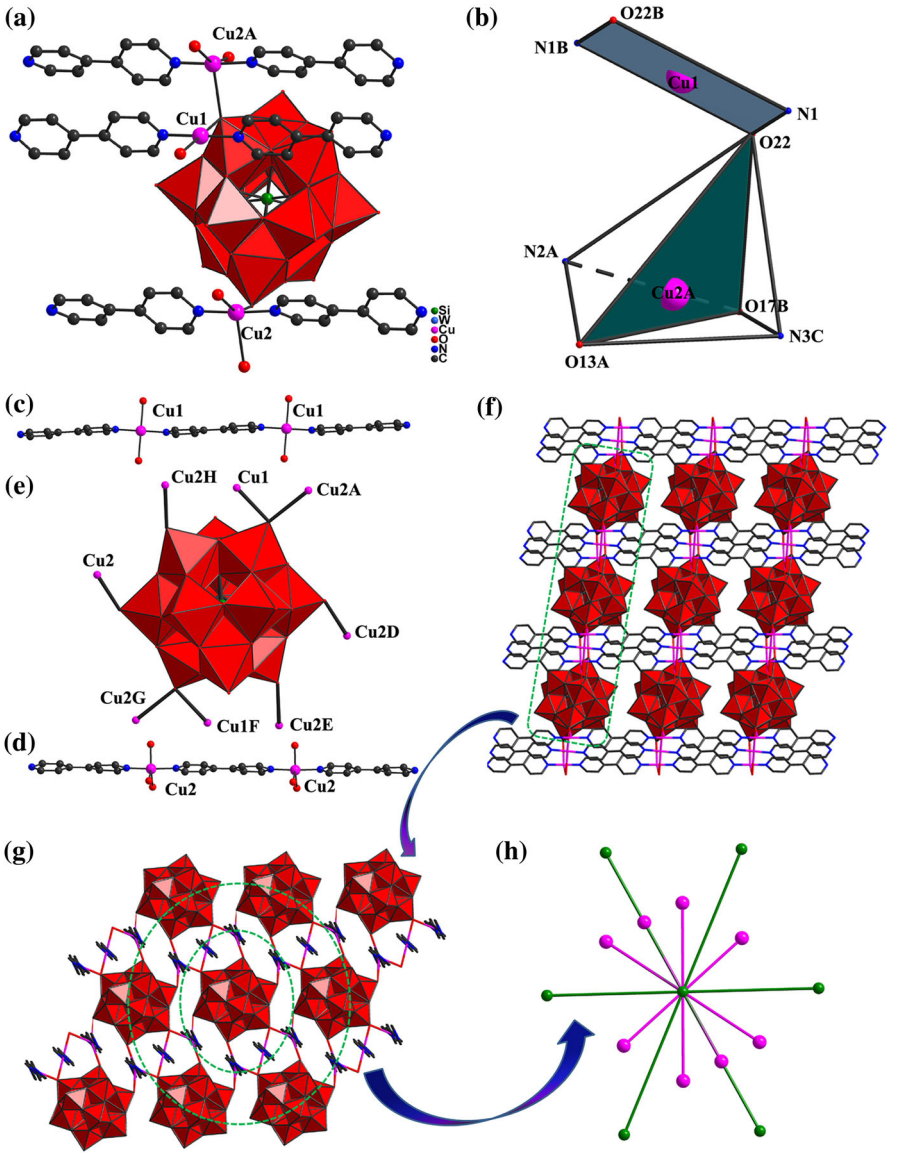

Fig. 2 **a** Combined ball-and-stick/polyhedral representation of the structural unit of **2** with the part labeling scheme. All the hydrogen atoms and water molecules are omitted for clarity. **b** Coordination environments of the $Cu1^{+}$ and $Cu2A^{+}$ cations. **c** The 1-D polymeric chains {–4,4′-bpy–Cu1–4,4′-bpy–Cu1–}$_n$. **d** The 1-D polymeric chains {–4,4′-bpy–Cu2–4,4′-bpy–Cu2–}$_n$. **e** The linking mode of $[\alpha\text{-SiW}_{12}O_{40}]^{4-}$ POA and Cu^{+} ions. **f** View of the 3-D extended framework of **2**. The atoms with "A, B, C, D, E" in their labels are symmetrically generated. Symmetry code: A: x, 1 + y, z; B: 1 − x, 3 − y, 1 − z; C: 1 + x, 1 + y, z; D: 1 − x, 2 − y, −z; E: x, y, −1 + z; F: x, −1 + y, −1 + z; G: 1 − x, 1 − y, −z; H: 1 − x, 2 − y, 1 − z. **g** The surroundings of each $[\alpha\text{-SiW}_{12}O_{40}]^{4-}$ POA with neighboring $[\alpha\text{-SiW}_{12}O_{40}]^{4-}$ POAs and Cu^{+} ions. **h** The simplified scheme of each $[\alpha\text{-SiW}_{12}O_{40}]^{4-}$ POA with neighboring $[\alpha\text{-SiW}_{12}O_{40}]^{4-}$ POAs and Cu^{+} ions

Author's personal copy

α-Keggin configuration. Similar to **1**, the Si center in the $[\alpha\text{-}SiW_{12}O_{40}]^{4-}$ POA in **2** is surrounded by eight half-occupied oxygen atoms displaying a distorted cubic geometry. There are two distinct copper coordination environments in the asymmetrical unit of **2**. The $[Cu1(4,4'\text{-bpy})]^{+}$ cation employs a slightly distorted square geometry, which is defined by two terminal O atoms from two $[\alpha\text{-}SiW_{12}O_{40}]^{4-}$ POAs [Cu–O: 2.81(2) Å] and two N atoms from two different 4,4′-bpy ligands [Cu–N: 1.91(2) Å]. The $[Cu2(4,4'\text{-bpy})]^{+}$ cation produces a five-coordinate trigonal bipyramid geometry built by three O atoms of three various $[\alpha\text{-}SiW_{12}O_{40}]^{4-}$ POAs [Cu–O: 2.79(2)–2.83(2) Å] occupying the equatorial plane position and two N atoms from neighboring two 4,4′-bpy ligands [Cu–N: 1.86(2)–1.89(2) Å] in the axis positions (Fig. 2b). Notably, two crystallographically unique copper cations in **2** are the +1 oxidation state, which can be confirmed by bond valance sum (BVS) calculation [58] [BVS values: Cu1: 1.39, Cu2: 1.42]. Obviously, the presence of Cu^{+} ions in the final product indicates that the starting Cu^{2+} ions are reduced by 4,4′-bpy or biim ingredients in the reaction process. Such phenomenon can be observed frequently in the hydrothermal reaction system containing N-donor ligands and the high oxidation state metals [59–62]. On the basis of the above-mentioned discussion, **1** and **2** show the flexible coordination modes of copper ion and convincingly prove that the POA clusters may be effectively used as inorganic building blocks in the design of organic–inorganic hybrid materials with high-dimensionalities, novel structures and unusual properties through the linkages of TM complexes.

The most striking structural feature of **2** is that two types of {–4,4′-bpy–Cu–4,4′-bpy–Cu–}$_n$ 1-D polymeric chains [namely, {–4,4′-bpy–Cu1–4,4′-bpy–Cu1–}$_n$ (Fig. 2c) and {–4,4′-bpy–Cu2–4, 4′-bpy–Cu2–}$_n$] (Fig. 2d) are connected together by hexadentate $[\alpha\text{-}SiW_{12}O_{40}]^{4-}$ POAs (Fig. 2e) that act as the inorganic bridging ligands, giving birth to the aesthetic 3-D extended architecture (Fig. 2f). Interestingly, each 4,4′-bpy ligand links two symmetrical Cu^{+} atoms into a {–4,4′-bpy–Cu–4,4′-bpy–Cu–}$_n$

1-D copper–organic polymeric chain and the neighboring {–4,4′-bpy–Cu–4,4′-bpy–Cu–}$_n$ polymeric chains are paralleled to each other and further linked together via the terminal oxygen atoms of the $[\alpha\text{-}SiW_{12}O_{40}]^{4-}$ POAs forming a regular grid possessing of the rectangular channels with the size of 10.89 × 3.66 Å (Fig. S1). Having an insight into the 3-D structure, each Cu1 ion grafts to the surface of two $[\alpha\text{-}SiW_{12}O_{40}]^{4-}$ POAs via two terminal oxygen atoms and the $[\alpha\text{-}SiW_{12}O_{40}]^{4-}$ clusters become pendants projecting toward two sides of the {–4,4′-bpy–Cu1–4,4′-bpy–Cu1–}$_n$ chain whereas each Cu2 ion links three $[\alpha\text{-}SiW_{12}O_{40}]^{4-}$ POAs that are located at different orientations toward the {–4,4′-bpy–Cu2–4,4′-bpy–Cu2–}$_n$. Another intriguing structural feature of **2** is that the $[\alpha\text{-}SiW_{12}O_{40}]^{4-}$ cluster is modified in an unusual linking mode (Fig. 2g,h), which is decorated by eight neighboring –Cu–4,4′-bpy–polymeric chains through six terminal oxygen atoms (O22, O17, O13, O22D, O17D, O13D), two of which are {–4,4′-bpy–Cu1–4,4′-bpy–Cu1–}$_n$ chains and the other six are {4,4′-bpy–Cu2–4,4′-bpy–Cu2–}$_n$ chains, and further grafted to six $[\alpha\text{-}SiW_{12}O_{40}]^{4-}$ clusters. Particularly, the terminal oxygen atoms O22 as well as O22A of $[\alpha\text{-}SiW_{12}O_{40}]^{4-}$ cluster are covalently bonding to two parallel {–4,4′-bpy–Cu–4,4′-bpy–Cu–}$_n$ chains, the linking mode of which is

Author's personal copy

interesting in POM chemistry. It is worth noting that eight {–4,4′-bpy–Cu–4,4′-bpy–Cu–}$_n$ polymeric chains are jointed together by a [α-$SiW_{12}O_{40}$]$^{4-}$ cluster to build up a "windmill" and the [α-$SiW_{12}O_{40}$]$^{4-}$ sphere located in middle position looks like the axis of the "windmill" (Fig. S2), which doubtlessly contributes to the significance of POMs in constructing the multi-dimensional framework. Furthermore, adjacent "windmills" are linked together by sharing eight {–4,4′-bpy–Cu–4,4′-bpy–Cu–}$_n$ chains to create the fascinating 3-D framework. As far as we know, Su and co-works reported a tri-track Cu–N chain modified Keggin POM {[Cu(4,4′-bipy)]$_3$[$HGeMo_{12}O_{40}$]}·0.5H_2O [63] and Niu et al. prepared a rail-like chain modified Keggin POM {[Cu^I(4,4′-bipy)]$_3H_2$(α-$BW_{12}O_{40}$)}·3.5H_2O [64]. In spite of the similarity that the connecting fashions between POM and {–4,4′-bpy–Cu–4,4′-bpy–Cu–}$_n$ chains, they have two obvious differences compared to **2,** which are described as follows: at first, the [$GeMo_{12}O_{40}$]$^{4-}$ POA acts as a tridentate inorganic ligand bonding to three {–4,4′-bpy–Cu–4,4′-bpy–Cu–}$_n$ chains and the [α-$BW_{12}O_{40}$]$^{5-}$ POA acts as a tetra-dentate inorganic ligand bonding to four {–4,4′-bpy–Cu–4,4′-bpy–Cu–}$_n$ chains while the [α-$SiW_{12}O_{40}$]$^{4-}$ POA is an octa-dentate inorganic ligand bonding to eight {–4,4′-bpy–Cu–4,4′-bpy–Cu–}$_n$ chains. Besides, {[Cu(4,4′-bipy)]$_3$ [$HGeMo_{12}O_{40}$]}·0.5H_2O shows a 1-D chain structure and {[Cu^I(4,4′-bipy)]$_3H_2$(α-$BW_{12}O_{40}$)}·3.5H_2O displays a 2-D sheet structure whereas **2** shows a 3-D extended structure. Soon afterwards, Niu's group discovered the first organic–inorganic hybrid 3-D 3d–4f heterometallic ST $(enH_2)_2${[Cu(en)$_2$(H_2O)][Cu(en)$_2$]$_2$Pr[(α-$H_{1.5}SiW_{11}O_{39}$)$_2$]}·6H_2O [65], in which each [Pr(α-$H_{1.5}SiW_{11}O_{39}$)$_2$]$^{10-}$ subunit acts as a penta-dentate ligand to join five [Cu(en)$_2$]$^{2+}$ groups to build up a fascinating 3-D architecture.

FT–IR Spectroscopy

The IR spectra of **1**, **2**, phen and 4,4′-bpy have been recorded on a Nicolet FT–IR 360 spectrometer in the region of 4000–400 cm^{-1} (Fig. 3), which is very useful for the identification of the characteristic vibration bands of the Keggin POAs and organic components. In the IR spectra of **1** and **2**, four characteristic bands derived from Keggin POAs are located at 970, 920, 883, 791 cm^{-1} in **1** and 973, 925, 887, 797 cm^{-1} in **2**, which are attributed to the ν_{as}(W–O_t), ν_{as}(Si–O_a), ν_{as}(W–O_b) and ν_{as}(W–O_c) of the [α-$SiW_{12}O_{40}$]$^{4-}$ POA, respectively. Compared with four characteristic vibration bands of K_4[α-$SiW_{12}O_{40}$]·17H_2O [66], the difference between them may mainly result from the non-ignorable interactions between [α-$SiW_{12}O_{40}$]$^{4-}$ POAs and $\left[Cu(phen)(H_2O)_2\right]^{2+}\Big/\left[Cu(phen)_2\right]^{2+}$ cations in **1** and [Cu(4,4′-bpy)]$^+$ cations in **2**. In addition, the obvious distinctions of IR spectra between **1**, **2** and Na_{10}[α-SiW_9O_{34}]·18H_2O (Fig. S3) are indicative of the structural conversion of [α-SiW_9O_{34}]$^{10-}$ to [α-$SiW_{12}O_{40}$]$^{4-}$. In comparison with the IR spectra of free phen and 4,4′-bpy, the appearance of vibration absorption bands at 1430 and 1520 cm^{-1} in **1** and 1421, 1527 and 1609 cm^{-1} denotes the presence of phen in **1** and 4,4′-bpy in **2**. The occurrence of resonance signals at 3435 cm^{-1} of **1** and 3482 cm^{-1} in **2** manifest the presence of coordination water molecules or lattice

Author's personal copy

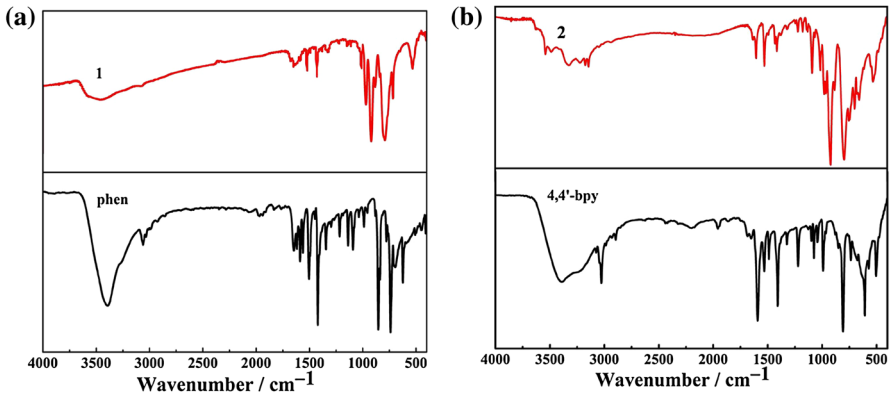

Fig. 3 IR spectra of **1** and **2**

water molecules. In short, the results of the IR spectra are in good agreement with the X-ray single-crystal analysis.

TG analysis

The TG curve of **1** was measured under a N_2 atmosphere on a Mettler − Toledo TGA/SDTA 851^e instrument at the heating rate of 10 °C min^{-1} (Fig. S4). It's evident that **1** undergoes two-step weight loss from 25 to 1000 °C. The first weight loss of 2.47 % occurs from 25 to 286 °C, roughly corresponding to the departure of four lattice water molecules and four two coordinated water molecules (calcd. 2.00 %). The second weight loss of 26.67 % continues to rise until 942 °C, which may be attributed to the removal of the phen ligand and the collapse of partial WO_3 in $[\alpha\text{-}SiW_{12}O_{40}]^{4-}$ framework, as WO_3 can be significantly sublimated upon 850 °C.

Electrochemical properties

Cyclic voltammetry (CV) experiments were performed to examine the electrochemical properties of **1**-CPE and **2**-CPE in the 0.5 mol·L^{-1} $H_2SO_4 + Na_2SO_4$ aqueous solution by entrapping them in CPEs since **1** and **2** were prepared by the hydrothermal reaction and were almost insoluble in water and also poorly soluble in common organic solvent. The CV figure of **1** in pH 5.02 sulfate medium (0.5 mol L^{-1} $Na_2SO_4 + H_2SO_4$) with the scan speed of 50 mV·s^{-1} at ambient temperature is shown in Fig. 4a, which can be clearly seen four groups of redox peaks I–I' (Ep_a = 0.038 V, Ep_c = –0.030 V), II–II' (Ep_a = –0.205 V, Ep_c = –0.312 V), III–III' (Ep_a = –0.672 V, Ep_c = –0.732 V) and IV–IV' (Ep_a = –0.871 V, Ep_c = –0.957 V) between –1.10 and 0.20 V with the half-wave potentials ($E_{1/2}$ = ($Ep_a + Ep_c$)/2, Ep_a and Ep_c are anodic and cathodic peak potentials) of 0.004 V, –0.259 V, –0.702 V and –0.914 V (vs the Ag/AgCl electrode). The I–I' redox peak

Author's personal copy

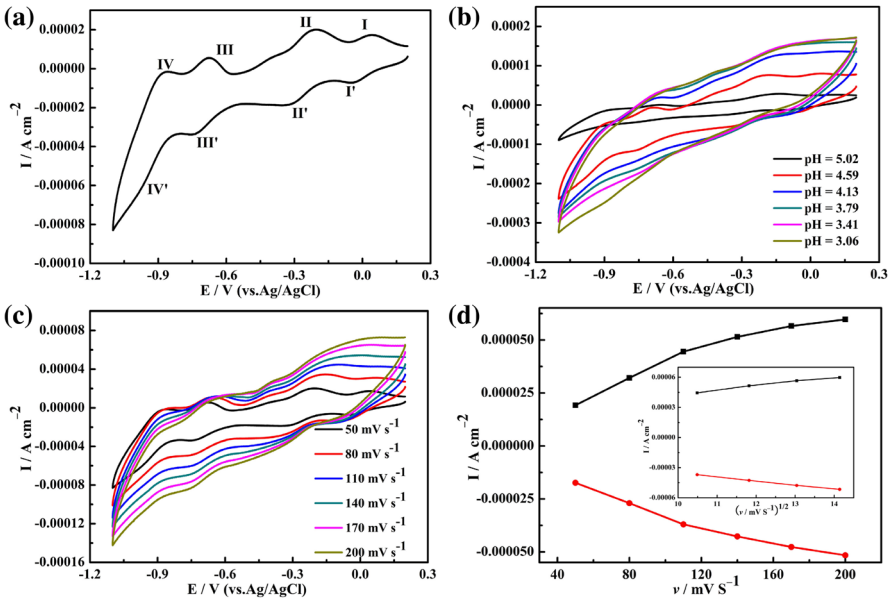

Fig. 4 **a** The cyclic voltammogram of **1**-CPE in the pH = 5.02 0.5 mol L^{-1} Na_2SO_4 + H_2SO_4 aqueous solution. Scan speed: 50 mV s^{-1}. **b** The variation of cyclic voltammograms of **1**-CPE with the pH value. **c** The cyclic voltammograms of **1**-CPE at variable scan speeds. **d** The relationship between cathodic peak currents (II) and scan speeds for **1**-CPE and the insets show the peak currents are proportional to the square root of the scan rates higher than 110 mV s^{-1}

is attributed to oxidation-reduction process of the Cu^{II} centers while the II–II', III–III' and IV–IV' redox peaks are assigned to the oxidation-reduction procedure of the W^{VI} centers in the $[\alpha\text{-}SiW_{12}O_{40}]^{4-}$ POAs [67, 68]. The peak-to-peak separations ΔE_p ($\Delta E_p = Ep_a – Ep_c$) for I–I', II–II', III–III' and IV–IV' are 0.068, 0.107, 0.060, 0.086 V, respectively, showing that I–I' and III–III' are reversible one-electron charge-transfer process whilst II–II' and IV–IV' are quasi-reversible one-electron charge-transfer process (the theoretical value of ΔE_p for a reversible one-electron charge-transfer process is about 59 mV) [69]. Besides, in order to probe into the influence of the acidity of the aqueous solution on the electrochemical response of **1**-CPE, the variation of CV of **1**-CPE with the pH value is recorded (Fig. 4b). The results manifest that the pH of the aqueous solution has an apparent effect on the electrochemical behavior of **1**-CPE. As the pH of the aqueous solution increases from 3.06 to 5.02, the CV patterns of W-waves are gradually shifted to the negative potential direction and the current intensities slowly decrease, which can be interpreted by the truth that the reduction of **1**-CPE is coupled with the evolution of protons from solution to the surface of the electrode to retain the charge neutrality [67]. As the pH value increases, comparatively slower penetration of protons to the surface of **1**-CPE should be the main reason for the current decrease and the negative shift of the reduction peak potential can be illuminated by the Nernst equation [67, 70]. Furthermore, the influence of the scan rate on the electrochemical behavior of **1**-CPE has been studied in the potential range of 0.2 to–1.1 V in the

Author's personal copy

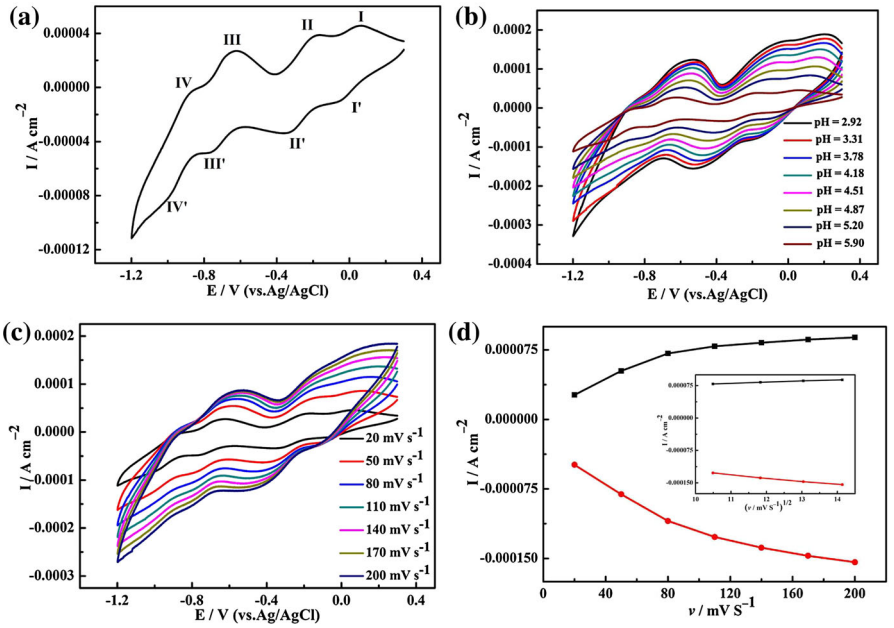

Fig. 5 **a** The cyclic voltammogram of **2**-CPE in the pH = 5.90 0.5 mol L^{-1} Na_2SO_4 + H_2SO_4 aqueous solution. Scan speed: 20 mV s^{-1}. **b** The variation of cyclic voltammograms of **2**-CPE with the pH value. **c** The cyclic voltammograms of **2**-CPE at variable scan speeds. **d** The relationship between cathodic peak currents (III) and scan speeds for **2**-CPE and the insets show the peak currents are proportional to the square root of the scan rates higher than 80 mV s^{-1}

abovementioned conditions and the scan rate varies from 50 to 200 mV s^{-1}. Figure 4c exhibits the evolution of the cathodic and anodic currents of the W-waves with different scan rates. Clearly, with the increase of the scan rate, the cathodic peak potential shifts towards the negative orientation while the corresponding anodic peak potential shifts to the positive orientation. As far as we know, the increase of the peak potential difference with increasing the scan rate is due to the fact that protons coming from solution diffuse into **1**–CPE to maintain the charge balance when **1**–CPE is reduced, thus the diffusion speed of protons into **1**–CPE largely determine the electrochemical reduction speed as the increase of the scan speed [71]. As shown in Fig. 4d, when the scan rate is lower than 110 mV s^{-1}, the peak current is proportional to the scan rate, indicating that the redox process is surface-controlled and the exchanging rate of electrons is fast. However, above 110 mV s^{-1}, the peak current is proportional to the square root of the scan rate, demonstrating that the redox process becomes diffusion-controlled [72].

Figure 5a illustrates the CV behavior of **2**-CPE in the pH 5.90 sulfate medium (0.5 mol L^{-1} Na_2SO_4 + H_2SO_4) at a scan rate of 20 mV·s^{-1} at room temperature in the potential range of –1.20 to 0.30 V. It's pretty evident that there exist three pairs of irreversible redox peaks I–I′ (Ep_a = 0.068 V, Ep_c = –0.046 V), II–II′ (Ep_a = –0.184 V, Ep_c = –0.325 V) and III–III′ (Ep_a = –0.633 V, Ep_c = –0.755 V) with the $E_{1/2}$ of 0.011 V, –0.254 V and –0.694 V (vs the Ag/AgCl electrode) and a pair

Author's personal copy

of quasi-reversible redox peak IV–IV′ (Ep_a = –0.876 V, Ep_c = –0.961 V) with the half-wave potential of –0.918 V. Obviously, The redox peaks of W^{VI} centers fragments resides in a more negative potential region than that of Cu^{I} centers and the II–II′, III–III′ and IV–IV′ redox peaks are attributed to the oxidation–reduction process of the W^{VI} centers in the $[\alpha\text{-}SiW_{12}O_{40}]^{4-}$ POAs [67, 68]. The ΔE_p for I–I' (0.114 V), II–II' (0.141 V), III–III' (0.122 V) and IV–IV' (0.085 V) indicates that I–I′, II–II′, III–III′ and IV–IV′ are one-electron charge-transfer process [69]. Moreover, the influence of the acidity of the aqueous solution as well as the scan rate on the electrochemical behavior of **2**-CPE have also been explored at room temperature. The CV patterns of W-waves change with the pH of the aqueous solution varying from 2.92 to 5.90, showing that the pH of the aqueous solution has an apparent influence on the electrochemical behavior of **2**-CPE (Fig. 5b). Besides, as the scan rate elevates from 20 to 200 mV s^{-1}, the cathodic peak potential moves to the negative direction and the anodic peak potential moves to the positive direction, but the midpoint potential hardly moved (Fig. 5c). Furthermore, the relationship between the peak current and the scan rate is liner when the scan rate is lower than 80 mV s^{-1}, revealing that the redox process of **2**-CPE is surface-controlled. Nevertheless, when the scan rate varies between 80 to 200 mV s^{-1}, the peak current has a liner relationship to the square root of the scan rate, declaring that the redox process becomes diffusion-controlled [72] (Fig. 5d). This influence of the scan rate on the electrochemical behavior of **2**-CPE makes us reminiscent of $(Hbpy)_4[SiMo_{12}O_{40}]$-CPE and $[Cu(bbi)]_5H[H_2W_{12}O_{40}]$-CPE reported by Peng and coworkers [73, 74].

Conclusions

In summary, two organic–inorganic hybrid STs $[Cu(phen)(H_2O)_2]_2[Cu(phen)_2]_2[\alpha\text{-}SiW_{12}O_{40}]_2{\cdot}4\ H_2O$ (**1**) and $[Cu(4,4\text{-}bpy)]_3H[\alpha\text{-}SiW_{12}O_{40}]{\cdot}3H_2O$ (**2**) have been hydrothermally synthesized and structurally characterized. **1** shows an infinite 1-D chain architecture constructed from alternate $[\alpha\text{-}SiW_{12}O_{40}]^{4-}$ POAs and $\{[Cu(phen)(H_2O)_2]^{2+}$ cations and $[Cu(phen)_2]^{2+}$ cations are appended to both sides of the 1-D chain. **2** displays an unprecedented 3-D framework built by $[\alpha\text{-}SiW_{12}O_{40}]^{4-}$ POAs and $[Cu(4,4'\text{-}bpy)_2]^{+}$ cations. The electrochemical properties of **1** and **2** are also studied at room temperature. In the following work, we will systematically tune the reaction conditions of lacuanry Keggin ST precursors, TM, Ln cations and rigid aromatic N-ligands to prepare novel organic–inorganic hybrid TM–Ln heterometallic STs with functional rigid aromatic N-ligands.

Supplementary Materials

Electronic Supplementary Information (ESI) available: Crystallographic data have been deposited with the Cambridge Crystallographic Data Center as supplementary publication CCDC 1049915 for **1** and 1049916 for **2**. These data can be obtained free of charge via www.ccdc.cam.ac.uk/data_request/cif, by emailing

Author's personal copy

data_request@ccdc.cam.ac.uk, or by contacting The Cambridge Crystallographic Data Centre, 12, Union Road, Cambridge CB2 1EZ, UK. Fax: C44 1223336033.

Acknowledgments This work was supported by the Natural Science Foundation of China (21101055, 213010 4 9, U130 4208), the Natural Science Foundation of Henan Province (12230 0 41010 6, 10230 0 410 093), the Foundation of State Key Laboratory of Structural Chemistry (20120 013), 2014 Special Foundation for Scientific Research Project of Henan University, 2012 Young Backbone Teachers Foundation from Henan Province and the Students Innovative Pilot Plan of Henan University (2013, 2014).

References

1. N. V. Izarova, M. T. Pope, and U. Kortz (2012). *Angew. Chem. Int. Ed.* **51**, 9492.
2. Q. X. Han, C. He, M. Zhao, B. Qi, J. Y. Niu, and C. Y. Duan (2013). *J. Am. Chem. Soc.* **135**, 10186.
3. M. T. Pope and A. Müller *Polyoxometalates: From Platonic Solids to Anti-Retroviral Activity* (Kluwer, Dordrecht, 1994).
4. D. L. Long, R. Tsunashima, and L. Cronin (2010). *Angew. Chem. Int. Ed.* **49**, 1736.
5. Y. C. Liu, F. C. Chun, S. T. Zheng, J. W. Zhao, and G. Y. Yang (2013). *Dalton Trans.* **42**, 16676.
6. Y. Wei, B. Xu, C. L. Barnes, and Z. Peng (2001). *J. Am. Chem. Soc.* **123**, 4083.
7. C. L. Lv, R. N. N. Khan, J. Zhang, J. J. Hu, J. Hao, and Y. G. Wei (2013). *Chem. Eur. J.* **19**, 1174.
8. S. T. Zheng and G. Y. Yang (2012). *Chem. Soc. Rev.* **41**, 7623.
9. P. J. Hagrman, D. Hagrman, and J. Zubieta (1999). *Angew. Chem. Int. Ed.* **38**, 2638.
10. C. L. Hill (1998). *Chem. Rev.* **98**, 1.
11. D. L. Long, E. Burkholder, and L. Cronin (2007). *Chem. Soc. Rev.* **36**, 105.
12. J. Hao, Y. Xia, L. S. Wang, L. Ruhlmann, Y. L. Zhu, Q. Li, P. C. Yin, Y. G. Wei, and H. Y. Guo (2008). *Angew. Chem. Int. Ed.* **47**, 2626.
13. B. S. Bassil, M. H. Dickman, I. Römer, B. Kammer, and U. Kortz (2007). *Angew. Chem. Int. Ed.* **46**, 6192.
14. U. Kortz, A. Tézé, and G. Hervé (1999). *Inorg. Chem.* **38**, 2038.
15. R. C. Howell, F. G. Perez, S. Jain, W. D. Horrocks, A. L. Rheingold, and L. C. Francesconi (2001). *Angew. Chem. Int. Ed.* **40**, 4031.
16. E. Cadot, M. A. Pilette, J. Marrot, and F. Sécheresse (2003). *Angew. Chem. Int. Ed.* **42**, 2173.
17. X. K. Fang, T. M. Anderson, and C. L. Hill (2005). *Angew. Chem. Int. Ed.* **44**, 3540.
18. J. W. Zhao, H. P. Jia, J. Zhang, S. T. Zheng, and G. Y. Yang (2007). *Chem. Eur. J.* **13**, 10030.
19. J. W. Zhao, J. Zhang, S. T. Zheng, and G. Y. Yang (2008). *Chem. Commun.* **44**, 570.
20. J. Thiel, C. Ritchie, C. Streb, D. L. Long, and L. Cronin (2009). *J. Am. Chem. Soc.* **131**, 4180.
21. K. Kamata, S. Yamaguchi, M. Kotani, K. Yamaguchi, and N. Mizuno (2008). *Angew. Chem. Int. Ed.* **47**, 2407.
22. U. Kortz, Y. P. Jeannin, A. Tézé, G. Hervé, and S. Isber (1999). *Inorg. Chem.* **38**, 3670.
23. S. G. Mitchell, P. I. Molina, S. Khanra, H. N. Miras, A. Prescimone, G. J. T. Cooper, R. S. Winter, E. K. Brechin, D. L. Long, R. J. Cogdell, and L. Cronin (2011). *Angew. Chem. Int. Ed.* **50**, 9154.
24. Z. M. Zhang, S. Yao, Y. G. Li, H. H. Wu, Y. H. Wang, M. Rouzières, R. Clérac, Z. M. Su, and E. B. Wang (2013). *Chem. Commun.* **49**, 2515.
25. M. Sadakane, M. H. Dickman, and M. T. Pope (2000). *Angew. Chem. Int. Ed.* **39**, 16.
26. J. P. Wang, J. W. Zhao, X. Y. Duan, and J. Y. Niu (2006). *Cryst. Growth Des.* **6**, 507.
27. S. Z. Li, D. D. Zhang, Y. Y. Guo, P. T. Ma, X. Y. Qiu, J. P. Wang, and J. Y. Niu (2012). *Dalton Trans.* **41**, 9885.
28. P. Mialane, L. Lisnard, A. Mallard, J. Marrot, E. A. Fidancev, P. Aschehoug, D. Vivien, and F. Sécheresse (2003). *Inorg. Chem.* **42**, 2102.
29. B. S. Bassil, M. H. Dickman, B. V. D. Kammer, and U. Kortz (2007). *Inorg. Chem.* **46**, 2452.
30. L. Ni, F. Hussain, B. Spingler, S. Weyeneth, and G. R. Patzke (2011). *Inorg. Chem.* **50**, 4944.

Author's personal copy

31. K. Suzuki, M. Sugawa, Y. J. Kikukawa, K. Kamata, K. Yamaguchi, and N. Mizuno (2012). *Inorg. Chem.* **51**, 6953.
32. W. L. Chen, Y. G. Li, Y. H. Wang, and E. B. Wang (2007). *Eur. J. Inorg. Chem.* **2007,** 2216.
33. Z. M. Zhang, Y. G. Li, W. L. Chen, E. B. Wang, and X. L. Wang (2008). *Inorg. Chem. Commun.* **11**, 879.
34. Z. M. Zhang, Y. G. Li, S. Yao, and E. B. Wang (2011). *Dalton Trans.* **40**, 6475.
35. S. Yao, J. H. Yan, Y. C. Yu, and E. B. Wang (2012). *Inorg. Chem. Commun.* **23**, 70.
36. H. H. Wu, S. Yao, Z. M. Zhang, Y. G. Li, Y. Song, Z. J. Liu, X. B. Han, and E. B. Wang (2013). *Dalton Trans.* **42**, 342.
37. B. Nohra, P. Mialane, A. Dolbecq, E. Rivière, J. Marrot, and F. Sécheresse (2009). *Chem. Commun.* **45,** 2703.
38. J. D. Compain, P. Mialane, A. Dolbecq, I. M. Mbomekallé, J. Marrot, F. Sécheresse, C. Duboc, and E. Rivière (2010). *Inorg. Chem.* **49**, 2851.
39. D. Y. Du, J. S. Qin, S. L. Li, Y. Q. Lan, X. L. Wang, and Z. M. Su (2010). *Aust. J. Chem.* **63**, 1389.
40. X. K. Fang, K. McCallum, H. D. Pratt III, T. M. Anderson, K. Dennisa, and M. Luban (2012). *Dalton Trans.* **41**, 9867.
41. H. Y. Zhao, J. W. Zhao, B. F. Yang, H. He, and G. Y. Yang (2013). *CrystEngComm* **15**, 8186.
42. H. J. Pang, C. J. Gómez-García, J. Peng, H. Y. Ma, C. J. Zhang, and Q. Y. Wu (2013). *Dalton Trans.* **42**, 16596.
43. S. W. Zhang, J. W. Zhao, P. T. Ma, H. N. Chen, J. Y. Niu, and J. P. Wang (2012). *Cryst. Growth Des.* **12**, 1263.
44. J. W. Zhao, J. Luo, L. J. Chen, J. Yuan, H. Y. Li, P. T. Ma, J. P. Wang, and J. Y. Niu (2012). *CrystEngComm* **14**, 7981.
45. J. Luo, C. L. Leng, L. J. Chen, J. Yuan, H. Y. Li, and J. W. Zhao (2012). *Synth. Met.* **162**, 1558.
46. S. W. Zhang, J. W. Zhao, P. T. Ma, J. Y. Niu, and J. P. Wang (2012). *Chem. Asian J.* **7**, 966.
47. J. Luo, J. W. Zhao, J. Yuan, Y. Z. Li, L. J. Chen, P. T. Ma, J. P. Wang, and J. Y. Niu (2013). *Inorg. Chem. Commun.* **27**, 2713.
48. A. Tézé and G. Hervé (1977). *Inorg. Chem.* **16**, 2115.
49. G. M. Sheldrick *SHELXS 97, program for crystal structure solution* (University of Göttingen, Göttingen, 1997).
50. G. M. Sheldrick *SHELXL 97, program for crystal structure refinement* (University of Göttingen, Göttingen, 1997).
51. J. W. Zhao, C. M. Wang, J. Zhang, S. T. Zheng, and G. Y. Yang (2008). *Chem. Eur. J.* **14**, 9223.
52. Z. M. Zhang, Y. G. Li, S. Yao, E. B. Wang, Y. H. Wang, and R. Clérac (2009). *Angew. Chem. Int. Ed.* **48**, 1581.
53. L. J. Chen, D. Y. Shi, J. W. Zhao, Y. L. Wang, P. T. Ma, and J. Y. Niu (2011). *Inorg. Chem. Commun.* **14**, 1052.
54. J. Y. Niu, Y. Shen, and J. P. Wang (2005). *J. Mol. Struct.* **733**, 19.
55. Y. Lu, Y. Xu, E. B. Wang, J. Lu, C. W. Hu, and L. Xu (2005). *Cryst. Growth Des.* **5**, 257.
56. M. X. Li, J. Du, J. P. Wang, and J. Y. Niu (2007). *Inorg. Chem. Commun.* **10**, 1391.
57. H. J. Pang, J. Peng, J. Q. Sha, A. X. Tian, P. P. Zhang, Y. Chen, and M. Zhu (2009). *J. Mol. Struct.* **922**, 88.
58. I. D. Brown and D. Altermatt (1985). *Acta Crystallogr. Sect.* **B41**, 244.
59. C. D. Wu, C. Z. Lu, H. H. Zhuang, and J. S. Huang (2002). *Inorg. Chem.* **41**, 5636.
60. C. M. Liu, D. Q. Zhang, and D. B. Zhu (2005). *Cryst. Growth Des.* **5**, 1639.
61. K. T. Potts, C. P. Horwitz, A. Fessak, M. Keshavarz-K, K. E. Nash, and P. J. Toscano (1993). *J. Am. Chem. Soc.* **115**, 10444.
62. H. Jin, Y. F. Qi, E. B. Wang, Y. G. Li, C. Qin, X. L. Wang, and S. Chang (2006). *Eur. J. Inorg. Chem.* **2006**, 4541.
63. J. Q. Sha, J. Peng, A. X. Tian, H. S. Liu, J. Chen, P. P. Zhang, and Z. M. Su (2007). *Cryst. Growth Des.* **7**, 2535.
64. J. W. Zhao, Y. P. Song, P. T. Ma, J. P. Wang, and J. Y. Niu (2009). *J. Solid. State Chem.* **182**, 1798.
65. S. W. Zhang, J. W. Zhao, P. T. Ma, H. N. Chen, J. P. Wang, and J. Y. Niu (2012). *Cryst. Growth Des.* **12**, 1263.
66. C. Rocchiccioli-Deltcheff, M. Fournier, R. Franck, and R. Thouvenot (1983). *Inorg. Chem.* **22**, 207.
67. X. L. Wang, E. B. Wang, Y. Lan, and C. W. Hu (2002). *Electroanal* **14**, 1116.
68. M. Sadakane and E. Stechhan (1998). *Chem. Rev.* **98**, 219.
69. N. Haraguchi, Y. Okaue, T. Isobe, and Y. Matsuda (1994). *Inorg. Chem.* **33**, 1015.

Author's personal copy

70. J. Wang *Analytical Electrochemistry* (VCH, New York, 1994).
71. Z. Han, Y. Zhao, J. Peng, Q. Liu, and E. Wang (2005). *Electrochim. Acta* **51**, 218.
72. Z. G. Han, Y. L. Zhao, J. Peng, Y. H. Feng, J. N. Yin, and Q. Liu (2005). *Electroanal* **17**, 1097.
73. P. P. Zhang, J. Peng, X. Q. Shen, Z. G. Han, A. X. Tian, H. J. Pang, J. Q. Sha, Y. Chen, and M. Zhu (2009). *J. Solid State Chem.* **182**, 3399.
74. Z. G. Han, Y. L. Zhao, J. Peng, Q. Liu, and E. B. Wang (2005). *Electrochim. Acta.* **51**, 218.